

Automatic Segmentation of the Brain and Intracranial Cerebrospinal Fluid in T_1 -Weighted Volume MRI Scans of the Head, and Its Application to Serial Cerebral and Intracranial Volumetry

Louis Lemieux,^{1,2*} Alexander Hammers,^{1–3} Toby Mackinnon,³ and Rebecca S.N. Liu^{1,2}

A new fully automatic algorithm for the segmentation of the brain and total intracranial cerebrospinal fluid (CSF) from T_1 -weighted volume MRI scans of the head, called *Exbrain v.2*, is described. The algorithm was developed in the context of serial intracranial volumetry. A brain mask obtained using a previous version of the algorithm forms the basis of the CSF segmentation. Improved brain segmentation is then obtained by iterative tracking of the brain–CSF interface. Gray matter (GM), white matter (WM), and intracranial CSF volumes and probability maps are calculated based on a model of intensity probability distribution (IPD) that includes two partial volume classes: GM-CSF and GM-WM. Accuracy was assessed using the Montreal Neurological Institute’s (MNI) digital phantom scan. Reproducibility was assessed using scan pairs from 24 controls and 10 patients with epilepsy. Segmentation overlap with the gold standard was 98% for the brain and 95%, 96%, and 97% for the GM, WM, and total intracranial contents, respectively; CSF overlap was 86%. In the controls, the Bland and Altman coefficient of reliability (CR) was 35.2 cm³ for the total brain volume (TBV) and 29.0 cm³ for the intracranial volume (ICV). Scan-matching reduced CR to 25.2 cm³ and 17.1 cm³ for the TBV and ICV, respectively. For the patients, similar CR values were obtained for the ICV. *Magn Reson Med* 49:872–884, 2003. © 2003 Wiley-Liss, Inc.

The segmentation of the brain from MRI scans has important applications in neuroimaging, in particular for the visualization and quantification of the cortex (1). Furthermore, the total brain volume has been shown to be correlated to various measures of disease severity (2,3), as have gray matter (GM) and white matter (WM) volumes (4). The intracranial volume is often used as a correcting factor, for example as an age- and/or gender-normalizing factor, to compare the volume of cerebral substructures between subjects (5). The segmentation of the cerebrospinal fluid (CSF) and the brain is also relevant to the quantitative analysis of morphological differences and changes due to neurological disorders (6). Segmentation of head scans

into GM, WM, and CSF can also be used to refine the quantitative analysis of magnetic resonance spectroscopy (MRS) and positron emission tomography (PET) by correcting for partial volume effects due to the mixture of tissues in each voxel (7,8). Finally, segmentation of head MRI scans is used in forward EEG and MEG modeling (9). Segmentation of the baseline image for the registration of serially acquired scans has been shown to be useful for measuring volume and signal changes with increased sensitivity (6,10–13).

Automated methods to segment the brain and the other intracranial tissues have generally relied on multiecho data and have used multispectral classification methods (14,15). Held et al. (16) demonstrated a method for segmenting GM, WM, and CSF based on Markov random fields in multiecho and proton density-weighted volume images. Methods applied to single-acquisition T_1 -weighted volume data have mainly focused on the segmentation of the GM and WM (17–19), the extraction of the brain as a whole (“scalping”) (20–22), or brain substructures (23). Methods for GM, WM, and CSF segmentation from T_1 -weighted volume MR scans have been described (24,25) but these require user intervention. Although the intervention may be trivial, this has the disadvantage of introducing subjectivity, and prevents batch processing of multiple datasets. To our knowledge, no fully automatic, validated method to segment both the brain and total intracranial CSF in T_1 -weighted volume scans has been reported yet.

In this work we describe and evaluate a new fully automatic method to segment the GM, WM, and CSF from T_1 -weighted volume data. It is an extension of, and incorporates, a previously published algorithm called *Exbrain* (22). We aimed to develop a tool that can be used as a data pipeline for batched processing, and therefore all steps in the new algorithm are completely automatic (no user intervention is required). We evaluate the method’s accuracy using a simulated MRI phantom scan, and its reproducibility using serially acquired T_1 -weighted volume MRI scans.

Segmentation Algorithm

The starting point of this work is the *Exbrain* brain segmentation (scalp removal) algorithm described in Ref. 22, with a few minor modifications (see next section); here we refer to this algorithm as “*Exbrain v.1*.” The output of *Exbrain v.1* is an image volume dataset containing the gray-level brain voxels surrounded by a null background, and constitutes the input of the new method presented

¹Epilepsy Research Group, Department of Clinical Neurology, Institute of Neurology, London, UK.

²MRI Unit, National Society for Epilepsy, Chalfont St. Peter, Buckinghamshire, UK.

³MRC Clinical Sciences Center and Division of Neuroscience, Faculty of Medicine, Imperial College, Hammersmith Hospital, London, UK.

Grant sponsor: Wellcome Trust.

*Correspondence to: Louis Lemieux, Ph.D., MRI Unit, National Society for Epilepsy, Chalfont St. Peter, Buckinghamshire SL9 0RJ, UK.
E-mail: l.lemieux@ion.ucl.ac.uk

Received 6 August 2002; revised 11 December 2002; accepted 11 December 2002.

DOI 10.1002/mrm.10436

Published online in Wiley InterScience (www.interscience.wiley.com).

© 2003 Wiley-Liss, Inc.

here. The combination of *Exbrain* v.1 and the new algorithm, which is implemented in a single computer program, constitutes *Exbrain* v.2.

As for *Exbrain* v.1, the new segmentation steps are based on a basic set of assumptions on the appearance of the head in T_1 -weighted volume scans. The assumptions are: 1) the WM constitutes a single connected component; 2) the WM is surrounded by a layer of GM, which has a lower intensity compared to WM; 3) the brain is surrounded by CSF, which has a lower intensity compared to GM; 4) no part of the brain or combined CSF and brain has a cross-section diameter less than approximately 5 mm. Implicit in these assumptions are the further assumptions of complete coverage of the head and a high spatial resolution (of the order of 1 mm).

Exbrain's output consists of the following: binary brain mask (volume: TBV_m); binary CSF mask (volume: $CSFV_m$); mean and standard deviation (SD) of GM, WM, and CSF voxel intensities; optimal CSF-GM threshold level; GMV; WMV; CSFV; and GM, WM, and CSF probability maps. The total brain volume (TBV) is the sum of GMV and WMV; the intracranial volume (ICV) is the sum of TBV and CSFV.

Improvements to *Exbrain* v.1

The brain histogram fitting used to determine the optimal GM and WM threshold level (steps 3 and 6) is now based on the tri-Gaussian model described below.

In step 2, the initial disconnection of the brain is now based on the calculation of the second moment of the spatial distribution of voxels, i.e., the mean square distance of each voxel to the center of mass, in the two largest objects identified by connectivity analysis. The most compact is labeled as "brain."

Data Preprocessing: Correction for Nonuniformity

For *Exbrain* v.1, we use the *N3* algorithm to remove signal nonuniformity due to RF inhomogeneity (26). *N3* is a fully automatic, self-contained package designed to maximize the global intensity histogram's high-frequency content by modeling the low-frequency spatial intensity variations. In a recent comparison (27) it was shown to perform at least as well as other published methods.

Intensity Probability Distribution (IPD)

Definitions

Three functions—the bi-Gaussian, tri-Gaussian, and penta-Gaussian distributions—are used to model the intensity distributions (histograms normalized to unity) of the voxels in various combinations of tissues, as described in the section on segmentation steps below. In the following, $\{A_i\} > 0$ and $\sum A_i = 1$. The bi-Gaussian is represented by the function $G_2(x; \mu_1, \sigma_1, A_1; \mu_2, \sigma_2, A_2)$, which is the sum of two Gaussians:

$$G_2(I; \mu_1, \sigma_1, A_1; \mu_2, \sigma_2, A_2) = A_1 G(I; \mu_1, \sigma_1) + A_2 G(I; \mu_2, \sigma_2). \quad [1]$$

Where I is voxel intensity, A_C is the total probability of tissue class "C," and μ_C and σ_C are the mean and SD, respectively, of the voxel intensity in tissue class "C."

The tri-Gaussian and penta-Gaussian have the same general form, with three and five Gaussians, respectively, and are represented by $G_3(I; \mu_1, \sigma_1, A_1; \mu_2, \sigma_2, A_2; \mu_3, \sigma_3, A_3)$ and $G_5(I; \mu_1, \sigma_1, A_1; \mu_2, \sigma_2, A_2; \mu_3, \sigma_3, A_3; \mu_4, \sigma_4, A_4; \mu_5, \sigma_5, A_5)$.

IPDs for Image Partitions

Following Ref. 24, we assume that the IPD of the brain, $P_{GM, WM}(I)$, can be modeled as a tri-Gaussian distribution: one each for GM and WM, and one for GM & WM partial volume voxels, which are modeled as consisting of 50% GM and 50% WM each. Therefore,

$$P_{GM, WM}(I) = G_3(I; \mu_{GM}, \sigma_{GM}, A_{GM}; \mu_{GMWM}, \sigma_{GMWM}, A_{GMWM}; \mu_{WM}, \sigma_{WM}, A_{WM}) = A_{GM} \times G(I; \mu_{GM}, \sigma_{GM}) + A_{WM} \times G(I; \mu_{WM}, \sigma_{WM}) + A_{GMWM} \times G(I; \mu_{GMWM}, \sigma_{GMWM}) \quad [2]$$

where GMWM represents the partial volume class, with:

$$\mu_{GMWM} = (\mu_{GM} + \mu_{WM})/2 \quad [3]$$

$$\sigma_{GMWM} = ((\sigma_{GM}^2 + \sigma_{WM}^2)/2)^{1/2}. \quad [4]$$

In a similar fashion, the IPD for the combined GM & CSF compartment is modeled as a tri-Gaussian:

$$P_{CSF, GM}(I) = G_3(I; \mu_{CSF}, \sigma_{CSF}, A_{CSF}; \mu_{CSFGM}, \sigma_{CSFGM}, A_{CSFGM}; \mu_{GM}, \sigma_{GM}, A_{GM}) \quad [5]$$

With:

$$\mu_{CSFGM} = (\mu_{CSF} + \mu_{GM})/2 \quad [6]$$

$$\sigma_{CSFGM} = ((\sigma_{CSF}^2 + \sigma_{GM}^2)/2)^{1/2}. \quad [7]$$

Finally, following Ref. 24, the IPD for the combined brain and CSF masks is modeled as a penta-Gaussian distribution, $P_{CSF, GM, WM}(I)$:

$$P_{CSF, GM, WM}(I) = G_5(I; \mu_{CSF}, \sigma_{CSF}, A_{CSF}; \mu_{CSFGM}, \sigma_{CSFGM}, A_{CSFGM}; \mu_{GM}, \sigma_{GM}, A_{GM}; \mu_{GMWM}, \sigma_{GMWM}, A_{GMWM}; \mu_{WM}, \sigma_{WM}, A_{WM}). \quad [8]$$

The partial volume intensity parameters μ_{CSFGM} , σ_{CSFGM} , μ_{GMWM} , and σ_{GMWM} are defined as in Eqs. [3], [4], [6], and [7]. In the following, the appropriate IPDs are fitted to the normalized intensity histograms within a given intensity range using the Simplex algorithm and the mean square difference as a cost function.

Exbrain v.2 Segmentation Steps

All operations are automatic and, except where explicitly stated otherwise, performed in 3D. The input data for the following algorithm are: nonuniformity corrected head

scan (I_{nuc} , from $N3$), segmented brain mask (I_{brain} ; with cut level at basis of cerebellum), fitted tri-Gaussian for GM & WM voxel intensities (μ_{GM} , σ_{GM} , μ_{WM} , σ_{WM}) and optimal GM-WM threshold level, $t_{\text{GM-WM}}$ (the latter three being outputs from *Exbrain* v.1).

Step 1: Segmentation of Intracranial CSF

The background is identified by 3D connected component analysis in I_{brain} .

For each slice in I_{brain} , a 2D connected component analysis is performed whereby all voxels of the brain's background that are not connected to the edges of the image are labeled "sulcal/ventricular" CSF, $\text{CSF}_{\text{s/v}}$.

Step 2: Initial CSF and Background Signal Intensity Characterization

The input volume, I_{nuc} , is processed using a median filter (spherical kernel, radius = 1.5 mm), giving $I_{\text{nuc}, m}$. The following operations are performed on $I_{\text{nuc}, m}$.

Following Ref. 28, the background noise is modeled as a Rayleigh distribution, and its mean, SD, μ_{BGND} , and σ_{BGND} are estimated from the random noise level, which we assume to be equal to the previously estimated mean of the GM and WM SDs, σ_{GMWM} . We obtain the following estimates of the background mean and SDs:

$$\mu_{\text{BGND}} = \sigma_{\text{GMWM}} \quad [9]$$

$$\sigma_{\text{BGND}} = 0.655\sigma_{\text{GMWM}}. \quad [10]$$

An initial histogram analysis of all sulcal/ventricular CSF is performed by fitting a tri-Gaussian, $G_3(I; \mu_{\text{CSF}}, \sigma_{\text{GM}}, A_{\text{CSF}}; \mu_{\text{CSFGM}}, \sigma_{\text{CSFGM}}, A_{\text{CSFGM}}; \mu_{\text{GM}}, \sigma_{\text{GM}}, A_{\text{GM}})$, with Eqs. [6] and [7] and $\sum A_i = 1$. Assuming that $\text{CSF}_{\text{s/v}}$ is principally made up of CSF and some CSF-GM partial volume voxels, and given that we are interested in estimating the CSF intensity, the intensity range is limited to the range, $[\mu_{\text{BGND}}, \mu_{\text{GM}}]$. Initialization of the parameters is as follows: μ_{CSF} is set to the position of the first peak in the histogram. σ_{CSF} is set to σ_{GM} and A_{CSF} to 0.2, $A_{\text{GM}} = 0$. If no peak is detected in the histogram, the $\text{CSF}_{\text{s/v}}$ mask is dilated (outside the brain mask, radius = 1.5 mm) and the histogram fitting operation is repeated. All tri-Gaussian parameters are kept fixed apart from μ_{CSF} , σ_{CSF} , A_{CSF} , and A_{GM} , giving initial estimates of μ_{CSF} and σ_{CSF} .

Step 3: Final CSF Segmentation

1. The optimal CSF-GM threshold level, $t_{\text{CSF-GM}}$, is calculated as follows from the $\text{CSF}_{\text{s/v}}$ histogram: First, an initial estimate of $t_{\text{CSF-GM}}$ is obtained algebraically (29) by assuming a bi-Gaussian, $G_2(I; \mu_{\text{CSF}}, \sigma_{\text{CSF}}, A_{\text{CSF}}, \mu_{\text{GM}}, \sigma_{\text{GM}}, A_{\text{GM}})$, giving $t_{\text{CSF-GM}0}$. Second, the effect of the CSF-GM partial volume class is then taken into account by adding the weighted mean intensity of the partial volume class:

$$t_{\text{CSF-GM}} = t_{\text{CSF-GM}0}(A_{\text{CSF}} + A_{\text{GM}}) + \mu_{\text{CSFGM}}A_{\text{CSFGM}}. \quad [11]$$

2. An optimal background-CSF threshold level, $t_{\text{BGND-CSF}}$, is derived algebraically by approximating the background-

CSF intensity distribution as a bi-Gaussian, $G_2(I; \mu_{\text{BGND}}, \sigma_{\text{BGND}}, 0.5, \mu_{\text{CSF}}, \sigma_{\text{CSF}}, 0.5)$ as above. The resulting $t_{\text{BGND-CSF}}$ defines the lower limit of the segmented CSF intensity.

The following operations are then performed on $I_{\text{nuc}, m}$:

3. Taking the initial brain mask as a starting point, a conditional dilation is performed with a spherical kernel radius of 1.5 mm and the following minimum and maximum thresholds: $[t_{\text{BGND-CSF}}, \mu_{\text{WM}} + 2.5 \times \sigma_{\text{WM}}]$. The difference between the resulting object and the brain mask is called the interface CSF mask. This step initializes the CSF mask to a single-voxel layer surrounding the brain; the wide intensity range is chosen to overcome imperfections in the brain mask, particularly superficial voxels lost due to morphological erosion operations used in *Exbrain* v.1.

4. An iterative conditional dilation operation is performed on the interface CSF mask with radius = 1.5 mm and the following minimum and maximum thresholds: $[t_{\text{BGND-CSF}}, t_{\text{GM-WM}}]$. This iterative intracranial filling process is stopped when the number of voxels added to the interface CSF mask at any step is zero.

5. Step 1 is repeated with the combined brain and CSF mask as input to identify residual sulcal/ventricular CSF, which is then added to the CSF mask.

Step 4: Refinement of the GM-CSF Boundary

The brain-CSF boundary in I_{nuc} is adjusted by iterative reclassification of voxels in a neighborhood (radius = 3 mm) of the voxels on the current GM-CSF interface. Only voxels that have an intensity lower than that of the kernel's central voxel are reclassified according to the rule:

$$\begin{aligned} C' &= C_{\text{CSF}} & \text{if } t_{\text{BGND-CSF}} \leq I < t_{\text{CSF-GM}} \\ C' &= C_{\text{GM}} & \text{if } I \geq t_{\text{CSF-GM}}. \end{aligned} \quad [12]$$

Where C' represents the new voxel classification. Voxels with $I < t_{\text{BGND-CSF}}$ are discarded from both the brain and CSF masks.

The iterative reclassification is terminated when the number of reclassified voxels is zero at a any step, in order to recover the brain voxels that may have been discarded in *Exbrain* v.1 due to erosion.

Step 5: Connectivity of Brain and Intracranial Compartments

a) First, the intracranial mask (sum of brain and CSF) is subjected to an opening operation, with radius = 3 mm, the largest connected component is identified, and all other components are discarded. The CSF and brain masks are then adjusted by masking both with the new intracranial mask.

b) Second, steps 3–5 of *Exbrain* v.1 are performed on the brain mask to discard voxels corresponding to marrow, dura, or sinuses that may have been reintroduced in step 4. The usefulness of this step was tested explicitly in our experiments.

c) Third, all voxels with $I > t_{\text{CSF-GM}}$ are discarded from the CSF mask.

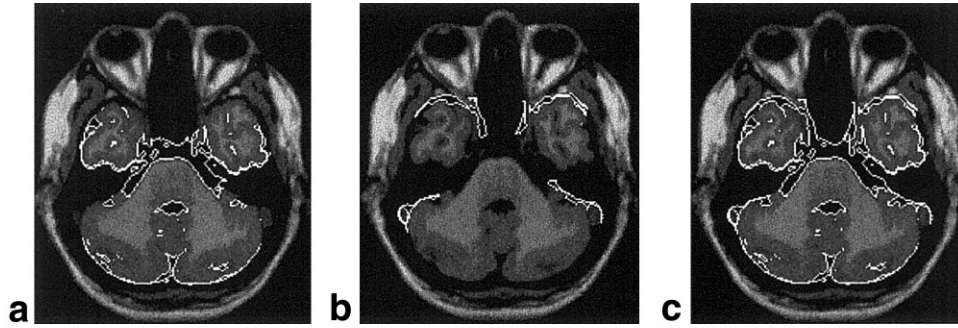


FIG. 1. Illustration of the CSF compartment in the MNI simulated brain scan with improvements. The white line represents the border of the CSF compartment. **a**: Outline of original CSF compartment obtained from the MNI *BrainWeb* website. **b**: CSF voxels contained in the original skin compartment and relabeled in this work (note that the relabeled voxels have the same intensity as the original CSF voxels). **c**: “Corrected” CSF compartment, which is the sum of the original CSF compartment and the CSF voxels contained in the skin and relabeled.

Step 6: Cutting in the Axial Plane

The brain and CSF masks are cut at the level of the basis of the cerebellum, as determined by *Exbrain* v.1.

Volumetry. The total number of voxels in the brain mask is TBV_m and the number of voxels contained in the CSF mask is $CSFV_m$. The total intracranial volume, ICV , is defined as

$$ICV = TBV_m + CSFV_m. \quad [13]$$

The final GMV, WMV, and CSFV estimates are calculated from the IPD as follows: The normalized histogram of the final combined brain and CSF mask is fitted to a penta-Gaussian, giving final estimates of the intensity parameters: μ_{CSF} , σ_{CSF} , μ_{GM} , σ_{GM} , μ_{WM} , σ_{WM} , and weights: A_{CSF} , A_{CSFGM} , A_{GM} , A_{GMWM} , and A_{WM} . Based on our model of the partial volume voxels, we then have:

$$GMV = ICV(A_{GM} + A_{CSFGM}/2 + A_{GMWM}/2) \quad [14]$$

$$WMV = ICV(A_{WM} + A_{GMWM}/2). \quad [15]$$

Finally, TBV is the sum of the new estimates of GMV and WMV, and $CVSF = ICV - TBV$.

Fuzzy Classification. Following Ref. 30, we implemented a fuzzy classification scheme, whereby a tissue fraction, f_i , for each tissue class (CSF, GM, and WM) is calculated for each voxel within the intracranial mask using the previously calculated class means, μ_i , as follows:

$$f_i = (I - \mu_i)^{-d} / \sum_k f_k \quad (i, k = CSF, GM, WM) \quad [16]$$

where I is the voxel intensity and d is an integer (here we chose $d = 2$). The special case $I = I_i$: then $f_i = 1$ and $f_j = 0$ ($j \neq i$); the fractional probabilities were multiplied by 255 for storage. This method was chosen because it is the one used for the *Brainweb* digital phantom, which is used for validation in the present work (see next section).

EXPERIMENTS

The algorithm’s accuracy was assessed in a first set of experiments using the Montreal Neurological Institute’s (MNI) *Brainweb* digital brain phantom (31). As described below, the *Brainweb* model was found to have clear imperfections and consequently required some editing before it could be used as a gold standard. Segmentation reproducibility was assessed in a second set of experiments by applying the segmentation to pairs of scans from 25 normal subjects and 11 patients with epilepsy. Performance was quantified based on a measure of voxel-by-voxel similarity and tissue volumes.

Digital Head Phantom and Simulated Scan

The MNI digital head phantom was used to assess the accuracy of the segmentation (31). The atlas is based on a digital anatomical model of normal brain, and consists of a partitioning of the head volume into 10 fuzzy tissue membership volumes (GM, WM, CSF, skull, fat, muscle/skin, skin, connective tissue, glial matter, and “other”), all of which are downloadable from <http://www.bic.mni.mcgill.ca/brainweb>. The GM, WM, glial matter (in effect, the CSF–WM interface, with an image intensity intermediate between GM and WM) and CSF true volumes are given as 902.9 cm³, 674.8 cm³, 6.0 cm³, and 371.9 cm³, respectively¹. Therefore, the reference values are TBV (sum of GM, WM, and glial matter) = 1583.7 cm³ and ICV (sum of brain and CSF) = 1955.6 cm³ (before correction; see below).

The *Brainweb* MRI volume simulator was then used to generate a realistic axial, T_1 -weighted volume head scan with $1 \times 1 \times 1$ mm³ voxels, 3% noise, and 20% nonuniformity.

Visual inspection of the downloaded CSF membership volume showed a significant number of erroneously labeled voxels. Inspection of the other membership volumes revealed that a significant amount of CSF had been as-

¹These are the “crisp” volumes listed on the Brainweb website (http://www.bic.mni.mcgill.ca/brainweb/anatomic_normal.html). The volumes for the fuzzy tissue membership volumes are: 898.9 cm³, 663.3 cm³, 6.3 cm³, and 370.8 cm³ for GM, glia, WM, and CSF, respectively.

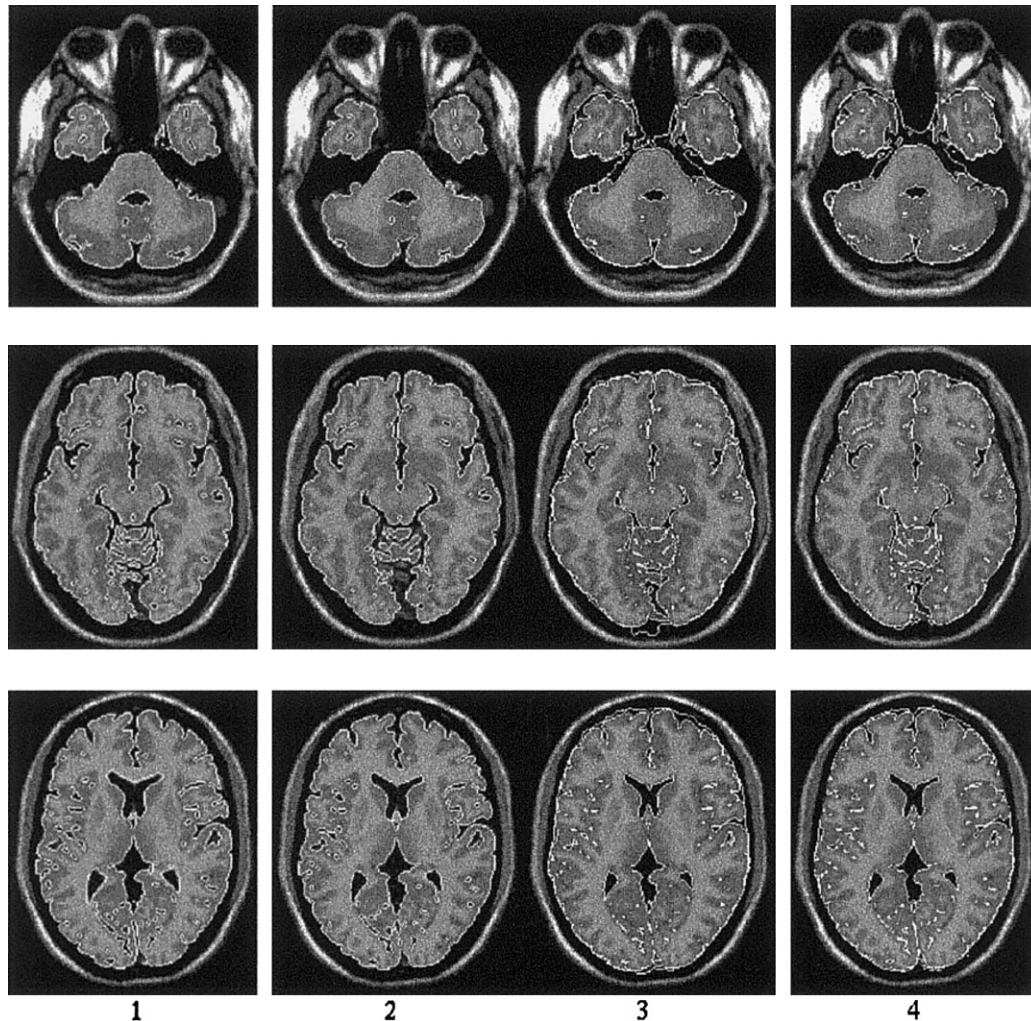


FIG. 2. Illustration of the automatic segmentation result for the *BrainWeb* simulated scan: binary brain and CSF masks. Three representative slices are shown. **Column 1:** Reference *BrainWeb* brain mask outline (sum of thresholded GM and WM fuzzy compartments). **Column 2:** *Exbrain* binary brain mask. **Column 3:** *Exbrain* binary CSF mask. **Column 4:** Reference *BrainWeb* CSF mask (thresholded CSF fuzzy compartment).

signed to the muscle-skin membership volume, particularly in the anterior, inferior aspect of the temporal lobes and cerebellum (see Fig. 1 for an illustration). The muscle-skin volume also includes the main draining veins.

Correction was performed using seeding and region-growing of the CSF voxels in the skin volume. A new, corrected CSF membership volume was obtained by adding the voxels thus identified to the original CSF volume (see Fig. 1). The resulting corrected CSF volume was 407.4 cm³, giving a corrected ICV of 1991.1 cm³.

The accuracy of the segmentation was assessed in two ways: 1) the volume of each compartment was compared to the given values, and 2) the degree of similarity between the segmentation result and the model was calculated as follows:

$$S_c = 2 \text{VOL}(S_{c,Exbrain} \cap S_{c,MNI}) / (\text{VOL}(S_{c,Exbrain}) + \text{VOL}(S_{c,MNI})).$$

Where $S_{c,Exbrain}$ is the binarized (by thresholding at 127) fuzzy classification mask for tissue or region “C” (GM,

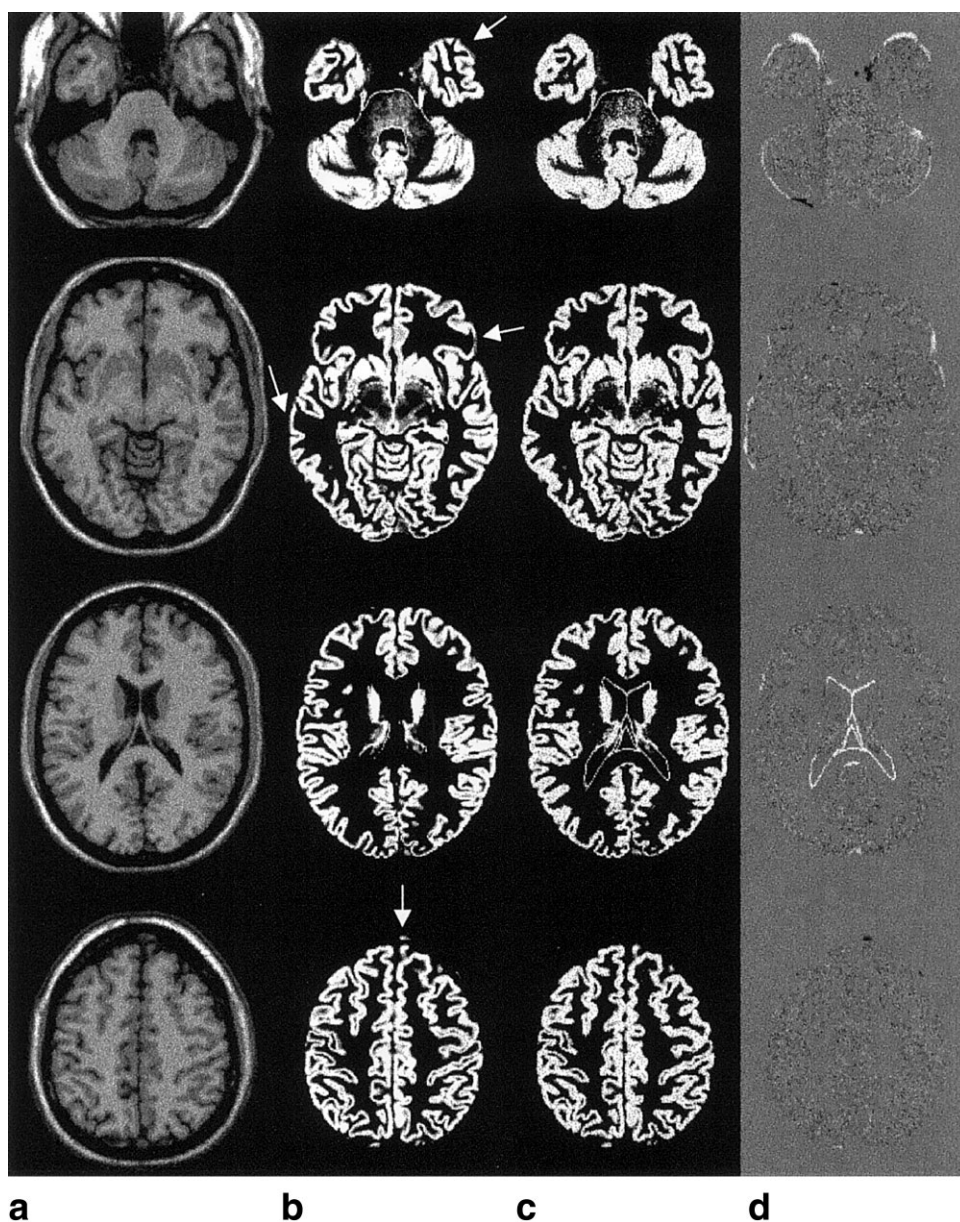
WM, CSF, brain, or intracranial tissue) obtained by segmentation and $S_{c,MNI}$ is the MNI mask for region “C,” also binarized by thresholding, and cut at the same level as the *Exbrain* segmentation. The brain and intracranial regions were obtained by adding the tissue probabilistic maps (GM and WM for brain, plus CSF for intracranial) followed by thresholding.

In view of the aforementioned uncertainty in the CSF gold standard, particularly in the inferior region, the quality of the ICV segmentation was evaluated over the whole intracranial region as automatically identified by *Exbrain* (the brainstem cut-level), and for the intracranial region above a point 3 cm higher than the brainstem cut-level, roughly corresponding to the base of the temporal lobes.

Scan Data

Twenty-five normal subjects (11 males and 14 females; mean age at baseline: 32.0 years, range: 22–57 years) and 11 patients (five males and six females; mean age at baseline: 31.1 years, range: 21–48 years) with chronic or newly diagnosed epilepsy were scanned twice. The mean scan

FIG. 3. Illustration of the automatic GM segmentation result for the *BrainWeb* simulated scan. **a**: Simulated scan. **b**: Reference GM compartment (binarized, threshold = 128). **c**: Binarized GM probability map obtained by segmentation (threshold = 128). **d**: Difference (**c** - **b**). The arrows indicate possible errors in the *BrainWeb* reference GM compartment.



interval was 8.2 months (range: 3.9–16.8 months) for the controls and 41.7 months for the patients (range: 41–42 months). Data from one control was discarded due to motion in the baseline scan, and data from one patient was rejected due to a large signal change in an abnormal vein between the two scans, leaving 24 control and 10 patient scan pairs for further analysis.

The scans were acquired using a fast, inversion recovery-prepared, spoiled gradient-recalled (IR-SPGR) T_1 -weighted volume sequence (TI/TR/TE = 450/15/4.2 ms, flip = 25°, matrix = 256 × 192, FOV = 24 × 18 cm, 124 1.5-mm-thick coronal slices) on a Signa 1.5T EchoSpeed MR imager (GE Medical Systems, Milwaukee, WI). This sequence is used in our routine protocol for morphometric analyses in patients with epilepsy (32). It represents a compromise between maximal coronal in-plane spatial resolution, whole-head coverage, suitability for 3D reconstruction and visualization, and scan time (6:56 min). In

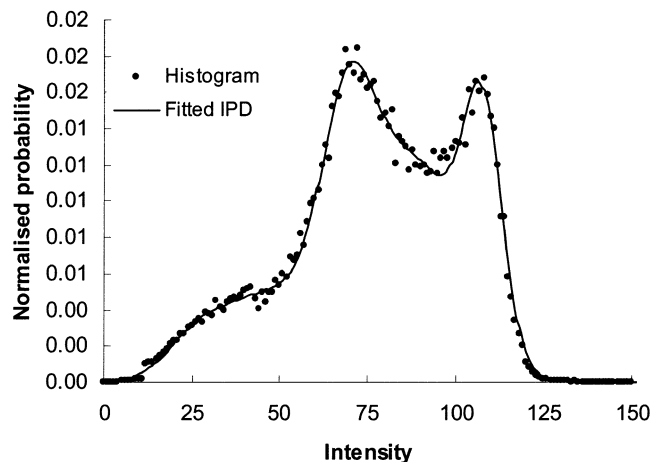


FIG. 4. Typical example of intracranial intensity histogram (dots) and fitted penta-Gaussian IPD (line) in a normal control subject.

Table 1
Baseline Intensity Probability Distribution (IPD)-Derived Volumes

Component	Controls		Patients	
	Mean volume (cm ³)	Range [Min-Max] (cm ³)	Mean volume (cm ³)	Range [Min-Max] (cm ³)
CSF	211.3	167.4–297.5	213.2	171.1–264.8
GM	743.9	646.9–889.4	771.3	645.4–874.4
WM	508.8	413.6–677.3	485.7	320.9–596.6
TBV	1252.7	1071.2–1566.7	1257.0	1067.2–1470.9
ICV	1464.1	1273.3–1864.2	1470.2	1246.5–1690.9

these images, typical tissue intensity characteristics are: $\mu_{GM} \approx 90$, $\mu_{WM} \approx 105$, $\sigma_{GM} \approx \sigma_{WM} \approx 4$, $\mu_{CSF} \approx 20$.

A dataset from a patient with chronic epilepsy was processed to test the applicability of the method to data with different characteristics, using the following acquisi-

tion parameters: IR-SPGR, T_1 -weighted volume sequence (TI/TR/TE = 600/9.7/4 ms, flip angle = 12, matrix size = 224×256 , FOV = 25.6 cm, 108 1.5-mm-thick sagittal slices) and the data were acquired on a 2T Magnetom system (Siemens). In this data, the approximate tissue

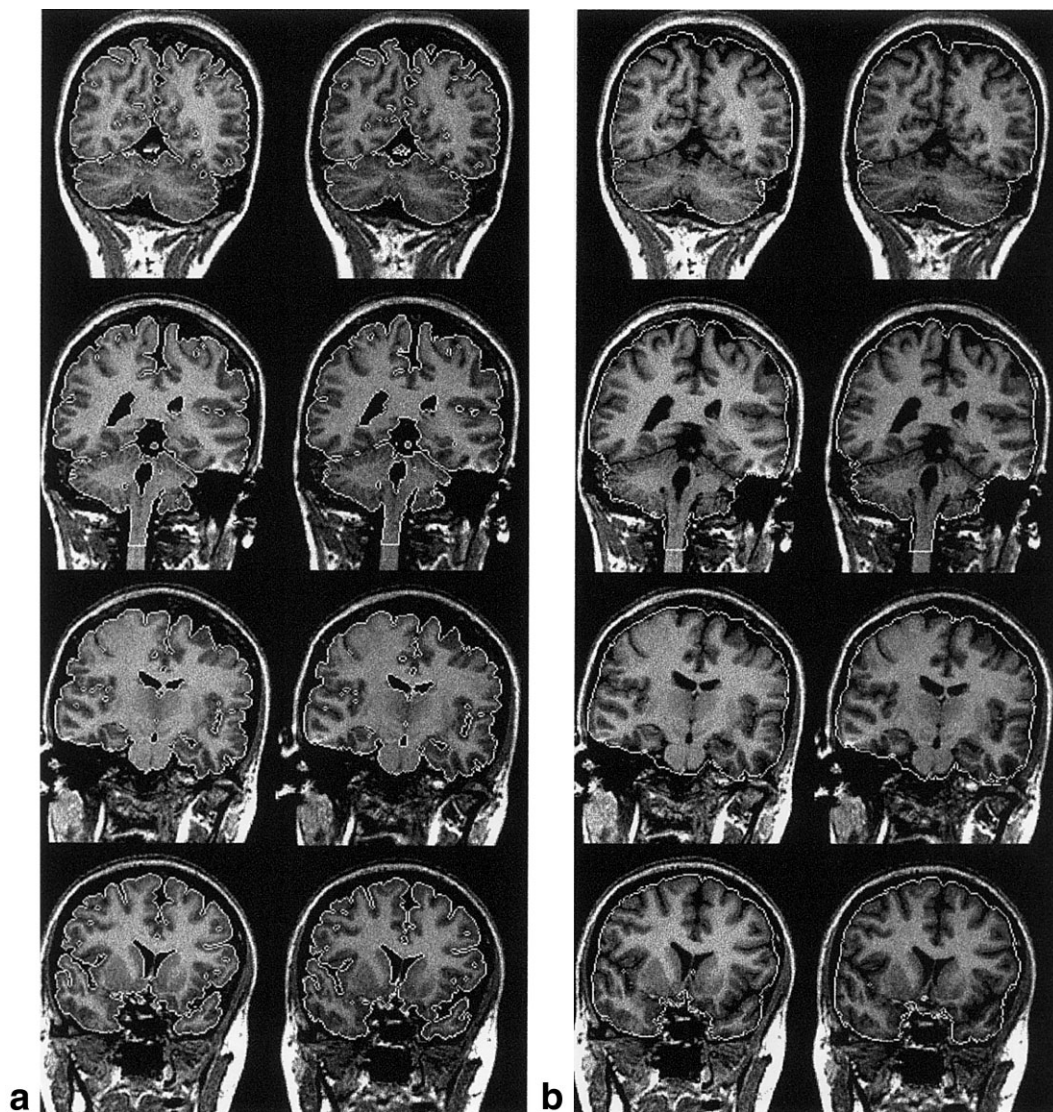


FIG. 5. Typical result of segmentation of a matched and registered scan pair from a normal control. **a:** Brain mask. **b:** Intracranial mask. Normal subject, a 30-year-old (at baseline) female. In this case $dTBV_m$ and $dTBV$ (registered and matched repeat minus baseline) were -0.88 cm^3 and -1.04 cm^3 , respectively, and $dICV$ was 7.06 cm^3 . Note the unorthodox orientation of the head, which did not affect the quality of the registration.

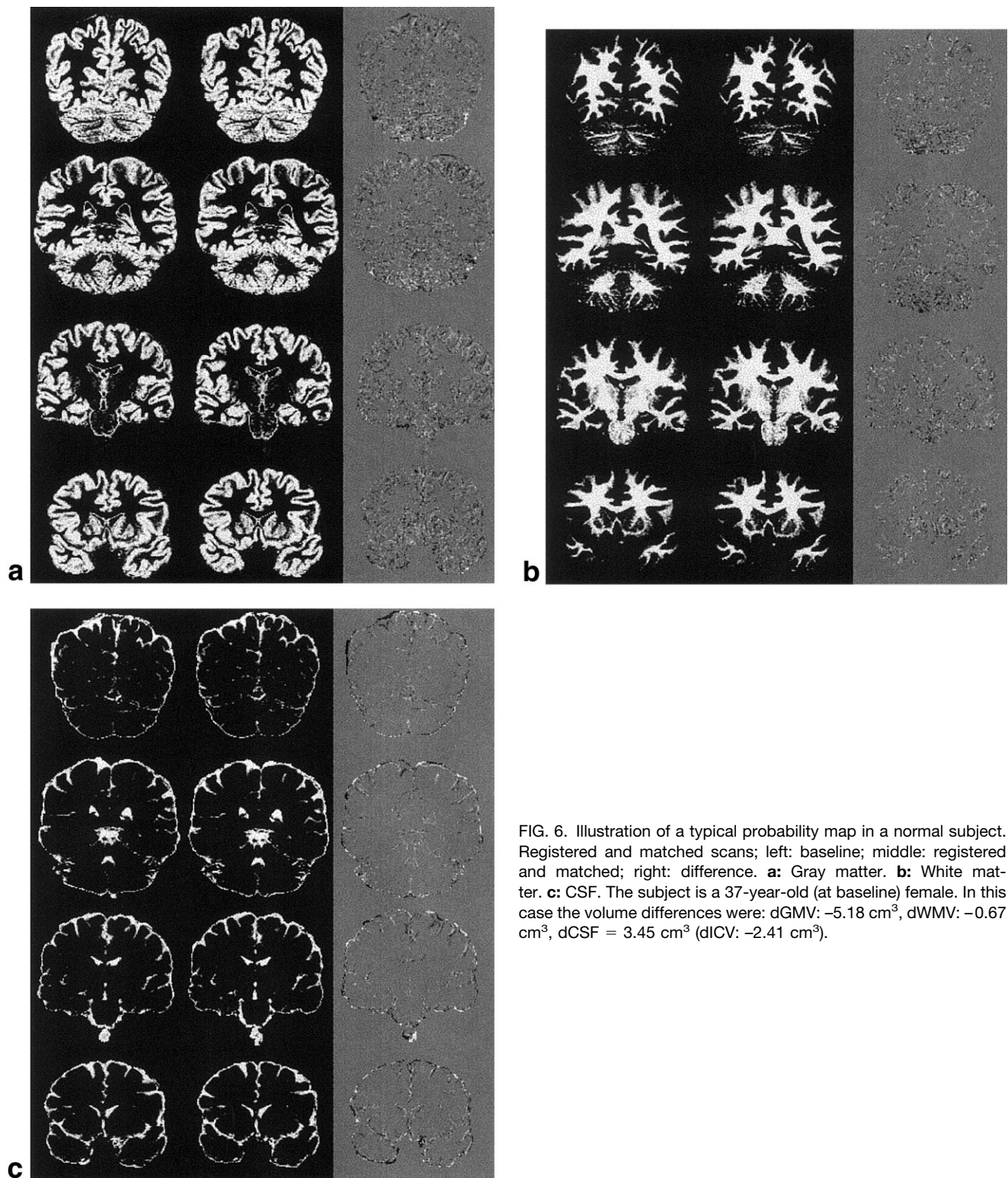


FIG. 6. Illustration of a typical probability map in a normal subject. Registered and matched scans; left: baseline; middle: registered and matched; right: difference. **a:** Gray matter. **b:** White matter. **c:** CSF. The subject is a 37-year-old (at baseline) female. In this case the volume differences were: $dGMV = -5.18 \text{ cm}^3$, $dWMV = -0.67 \text{ cm}^3$, $dCSF = 3.45 \text{ cm}^3$ ($dICV = -2.41 \text{ cm}^3$).

intensity characteristics were: $\mu_{GM} \approx 850$, $\mu_{WM} \approx 950$, $\sigma_{GM} \approx \sigma_{WM} \approx 50$, $\mu_{CSF} \approx 300$.

Reproducibility

Reproducibility was assessed by calculating the mean and SD of the difference between the tissue volumes obtained

by segmenting the baseline and repeat scans. We also wanted to determine the effect of scan registration on the segmentation reproducibility. The baseline scan was segmented and the repeat scan registered to the baseline based on a nine-parameter (three rotation, three translation, and three scaling) affine transformation by iteratively maximizing the intensity cross-correlation within the

Table 2
IPD-Derived Tissue Volume Changes in 20 Normal Controls Scanned 8.2 Months Apart

	dGMV		dWMV		dTBV ^a		dCSFV		DICV ^b	
	Mean	CR	Mean	CR	Mean	CR	Mean	CR	Mean	CR
cm ³										
Repeat-baseline	+0.83	24.0	+0.98	25.4	+1.82	35.2	+0.58	22.0	+2.39	29.0
Registered repeat-baseline	+2.72	26.4	+0.51	20.2	+3.24	24.2	+1.36	25.8	+4.59	20.8
Registered and matched repeat-baseline	+7.77	29.0	-3.96	9.50	+3.81	25.2	+0.75	24.0	+4.56	17.1
% of baseline volume										
Repeat-baseline	+0.10	3.06	+0.19	5.0	+0.15	2.80	+0.27	10.42	+0.16	1.98
Registered repeat-baseline	+0.35	3.36	+0.10	3.98	+0.26	1.94	+0.64	12.20	+0.31	1.42
Registered and matched repeat-baseline	+0.99	3.70	-0.77	1.86	+0.30	2.02	+0.35	11.36	+0.31	1.16

^aTBV is the sum of GMV and WMV.

^bICV is the sum of TBV and CSFV. CR, Coefficient of repeatability = $2 \times \text{SD}$.

baseline brain mask² (10,33). Reslicing was performed using sinc interpolation (kernel radius = 5). The registered repeat scan was segmented and the ratio of the mean registered to baseline intensities within the baseline brain mask was recorded:

$$R = \langle I_{\text{registered}} \rangle / \langle I_{\text{baseline}} \rangle.$$

Finally, the registered repeat scan was segmented twice, once without and once with the intensity correction factor, R , taken into account. In the latter the segmentation and volumetric calculations were modified to use knowledge derived from the baseline segmentation in an attempt to improve reproducibility. First, the following values from the baseline scan segmentation, adjusted by multiplying by R , were used as input and kept fixed throughout segmentation: 1) foreground threshold level (*Exbrain* v.1), 2) background-CSF threshold level, $t_{\text{BGND-CSF}}$, and 3) level of the brainstem cut. Second, in the final volumetric calculation, the starting penta-Gaussian parameter values were set to the final estimates obtained for the baseline scan, also multiplied by R , with the mean intensities (μ_{CSF} , μ_{GM} , μ_{WM}) and SDs (σ_{CSF} , σ_{GM} , σ_{WM}) kept fixed and the following parameters estimated: A_{CSF} , A_{CSFGM} , A_{GM} , A_{GMWM} , and A_{WM} .

We use the coefficient of repeatability (CR), twice the SD of the difference, as a measure of reproducibility (34). The coefficient of variation (CV), defined as the absolute difference between repeated values expressed as a percentage of baseline, is commonly used to express reproducibility (35). Therefore, we also calculated the CV and expressed the CR as a percentage of baseline to facilitate comparisons.

RESULTS

Accuracy

Figures 2 and 3 illustrate the result of the automatic segmentation of the MNI simulated scan. The similarity was 0.977, 0.860, and 0.964 for the binary brain, CSF, and intracranial masks (combined brain-CSF) segmentations,

respectively. The similarity for the GM and WM probability maps was assessed by first applying a threshold of 128 on the maps and calculating similarity with the thresholded MNI reference GM and WM maps; the results were 0.945 and 0.964, respectively. The similarity for the intracranial mask with a higher brainstem cut level was 0.966.

A visual comparison of the brain and CSF segmentation and the gold standard revealed that the error consisted of isolated voxel clusters distributed roughly uniformly around the brain, with occasional erroneous inclusion of sinuses in the *Exbrain* CSF mask. With regard to the GM segmentation, Fig. 3 shows misclassification of the ventricular WM-CSF interface as GM, and apparent clusters of surplus GM, for example around the antero-inferior and lateral aspects of the temporal lobes. The former results from classification based on intensity alone, and can be addressed using voxel neighborhood information (see Discussion). The latter indicates errors in the reference tissue models, upon inspection of the temporal lobes in the simulated data, as indicated by the arrows (Fig. 3).

The TBV and ICV values calculated using *Exbrain* were 1586.6 cm³ and 1965.5 cm³, representing errors of +0.1% and -1.3%, respectively, compared to the reference TBV and corrected ICV fuzzy volumes (+0.5% relative to the uncorrected ICV). The GM, WM, and CSF volumes were 921.5 cm³, 665.1 cm³, and 378.9 cm³, respectively, corresponding to errors of +2.0%, -1.4%, and -5.0%, respectively, relative to the reference values (corrected, in the case of CSF; error is +1.8% relative to uncorrected CSF). The binary mask volumes, TBV_m and CSF_m, were 1541.5 cm³ and 424.0 cm³, corresponding to errors of -2.3% and +4.1%, respectively.

Reproducibility

The average time taken for the complete segmentation process of the real scans was 10 min on a SunBlade 1000 Unix workstation (SUN Microsystems, Palo Alto, CA) with 512MB RAM.

Normal Control Data

The mean values for the fitted histogram mean intensities and SDs for each tissue class were: $\mu_{\text{CSF}} = 25.5$, $\sigma_{\text{CSF}} = 8.2$;

²The scaling parameters are used to correct for changes in voxel dimensions; see Ref. 33.

Table 3
Binary Brain and CSF Mask Volume Changes in 20 Normal Controls Scanned 8.2 Months Apart

	dT _{BM}		dCSF _m	
	Mean	CR	Mean	CR
cm ³				
Repeat-baseline	+2.36	40.62	+0.03	33.58
Registered repeat-baseline	+8.47	34.54	-3.88	36.00
Registered and matched repeat-baseline	+2.69	24.30	+1.86	23.20
% of baseline volume				
Repeat-baseline	+0.19	3.24	+0.00	15.88
Registered repeat-baseline	+0.67	2.76	+1.83	17.02
Registered and matched repeat-baseline	+0.21	1.94	+0.88	10.96

CR, Coefficient of repeatability = $2 \times \text{SD}$.

$\mu_{\text{GM}} = 75.6$, $\sigma_{\text{GM}} = 8.8$; $\mu_{\text{WM}} = 111.7$, $\sigma_{\text{WM}} = 5.8$; $\mu_{\text{CSF-GM}} = 50.6$, $\sigma_{\text{CSF-GM}} = 8.5$; and $\mu_{\text{GM-WM}} = 93.7$, $\sigma_{\text{GM-WM}} = 7.5$. Figure 4 illustrates a typical intensity histogram and fitted IPD in a normal control subject. In this case the cross-correlation between the two curves is 0.997. The mean final values for the threshold levels used in the algorithm were: $t_{\text{BGND-CSF}} = 11$, $t_{\text{CSF-GM}} = 48$, $t_{\text{GM-WM}} = 95$.

The mean baseline IPD-derived volumes are shown in Table 1. The mean proportion of partial volume voxels were: $A_{\text{CSF-GM}} = 0.20$ and $A_{\text{GM-WM}} = 0.34$. The mean baseline brain and CSF mask volumes were: $\text{TBV}_m = 1252.6 \text{ cm}^3$ and $\text{CSF}_m = 211.6 \text{ cm}^3$. The correlation coefficient between TBV and TBV_m was 0.997. Figures 5 and 6 illustrate typical segmentation results for the baseline and matched repeat scans.

The repeat-baseline volume differences were found to be uncorrelated to the baseline values (Pearson correlation = 0.06). The results for GMV, WMV, CSFV, TBV, and ICV are summarized in Table 2, and the results for TBV_m and CSFV_m are summarized in Table 3. These show that registration alone improves the reproducibility of TBV, ICV, and TBV_m . Intensity matching following registration does not result in any substantial improvement, except for the TBV_m and CSF_m , which show a substantial drop in both the mean and SD of the difference.

For comparison purposes, the mean CV for GMV, WMV, CSFV, TBV, and ICV for the repeat-baseline comparison are: 1.32%, 2.09%, 4.26%, 1.12%, and 0.81%, respectively.

Patient Data

The mean baseline IPD-derived volumes are shown in Table 1. There were no baseline volume group differences between patient and controls. The mean baseline binary brain and CSF mask volumes were: $\text{TBV}_m = 1257.3 \text{ cm}^3$ and $\text{CSF}_m = 212.9$. The reproducibility results are summarized in Tables 4 and 5. Figure 7 illustrates the segmentation for a patient with chronic epilepsy. The difference image shows the usual signs of atrophy, in particular a dark rim around the ventricles.

DISCUSSION AND CONCLUSIONS

We have demonstrated and validated a fully automatic algorithm for the segmentation of brain tissues and total intracranial CSF in T_1 -weighted volume scans. Our approach is based on a combination of morphological operations and intensity thresholds, guided by a basic set of assumptions on the appearance of the head in T_1 -weighted volume scans.

The algorithm's relative complexity is its principal weakness, as it may appear to be specifically designed for our own data. However, the algorithm contains no explicit reference to scan orientation, apart from the brainstem cutting step, which relies on accurate header information. We have not systematically evaluated the method's robustness for different scanners or other scan orientations; however, Fig. 8 shows evidence for the general validity of our approach. Our substantial (albeit anecdotal) experience

Table 4
IPD-Derived Tissue Volume Changes in 10 Patients With Epilepsy Scanned 3.5 Years Apart

	dGMV		dWMV		dT _{BV} ^a		dCSFV		DICV ^b	
	Mean	CR	Mean	CR	Mean	CR	Mean	CR	Mean	CR
cm ³										
Repeat-baseline	-11.09	40.34	-14.07	36.88	-25.16	72.38	+17.03	44.08	-8.13	34.48
Registered repeat-baseline	+6.86	27.74	-3.00	25.02	+3.85	47.46	+6.66	59.60	+10.52	21.26
Registered and matched repeat-baseline	-4.81	59.14	-11.45	27.18	-16.31	48.50	+24.80	42.66	+8.49	18.76
% of baseline volume										
Repeat-baseline	-1.44	5.24	-2.90	7.60	-2.00	5.76	+7.99	20.68	-0.55	2.34
Registered repeat-baseline	+0.89	3.60	-0.62	5.16	+0.31	3.94	+3.13	27.76	+0.72	1.44
Registered and matched repeat-baseline	-0.63	7.66	-2.36	5.60	-1.30	3.86	+11.63	20.02	+0.58	1.28

^aT_{BV} is the sum of GMV and WMV.

^bICV is the sum of TBV and CSFV. CR, Coefficient of repeatability = $2 \times \text{SD}$.

Table 5
Binary Brain and CSF Mask Volume Changes in Patients With Epilepsy Scanned 3.5 Years Apart

	dTBV _m		dCSFV _m	
	Mean	SD	Mean	SD
cm ³				
Repeat-baseline	-27.90	101.82	+19.78	77.16
Registered repeat-baseline	+2.37	79.06	+8.15	91.42
Registered and matched repeat-baseline	-9.31	52.34	+17.81	46.78
% of baseline volume				
Repeat-baseline	-2.22	8.10	+9.29	36.24
Registered repeat-baseline	0.19	6.28	+3.83	42.94
Registered and matched repeat-baseline	-0.74	4.16	+8.36	21.96

with segmenting T_1 -weighted volumetric scans from other centers indicates that performance is generally a reflection of accuracy of the header information and image quality; noise (intrinsic, motion, etc.), contrast (CSF-background), spatial resolution, and preprocessing. The algorithm generally performs less well on data that has been interpolated, due to blurring.

Validation relied on a widely used synthetic “gold standard” for accuracy, and on repeated scans for reproducibility.

The similarity with the MNI gold standard was 98% for the brain and 96–97% for the intracranial volume (depending on the inferior cut level). In terms of total volume, the results for both structures revealed an excellent agreement with the given values, with errors of 1.3% or less. Our finding that the segmentation similarity is higher for the brain than for combined brain-CSF reflects the difficulty of segmenting the latter. This is likely due to a combination of the following factors: the low signal-to-

noise ratio (SNR) of the CSF, and its thinness and convolutedness (particularly in the skull base, which makes it more subject to the partial volume effect and therefore more difficult to segment using morphological operations). Indeed, comparison of the results for the higher brainstem cut level is consistent with this observation. Visual inspection of the automatic CSF segmentation result revealed that the error was uniformly distributed around the cranial vault. GM and WM segmentation (not shown) was in good agreement with the reference maps, and we provided evidence of consistent results in repeated scans. Our results for GM and WM segmentation are slightly worse than those obtained by Grabowski et al. (24) in terms of volume, although we have shown some deficiencies in the reference data.

The accuracy of segmentation of the CSF (steps 2 and 3) without median filtering was much inferior to the results reported here (results not shown). Regarding the utility of step 5b, which may be considered rather ad hoc, it is

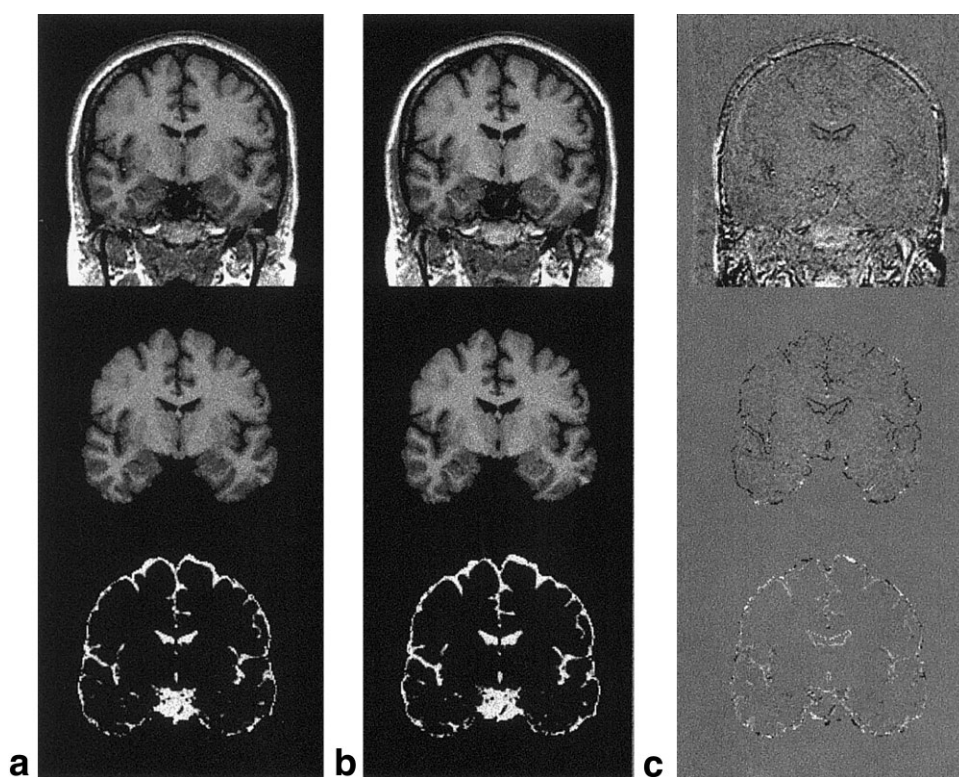


FIG. 7. Illustration of the segmentation for a 34-year-old female with a history of chronic epilepsy. Top row: registered and matched scans; middle row: brain segmentation (binary mask applied to image); bottom row: CSF probability maps. **a:** Baseline. **b:** Registered and matched repeat scan. **c:** Difference image (registered and matched repeat scan minus baseline). A dark rim can be seen in the brain mask difference image, indicative of cerebral volume loss. A bright rim around the brain and the ventricles can be seen in the CSF difference image, indicative of CSF volume increase. In this case, dTBV_m was -27.0 cm³, dCSF_m was +30.6 cm³, and dICV was +3.6 cm³.

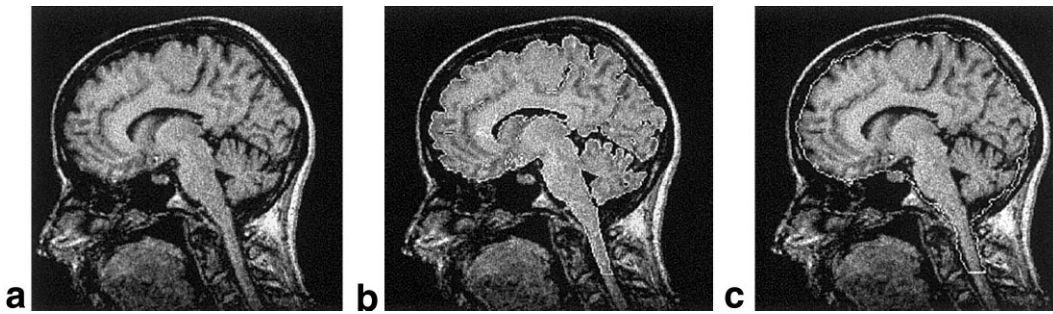


FIG. 8. Illustration of the segmentation result for the sagittal scan acquired on the 2T Siemens scanner: (a) slice from original data, (b) with binary brain mask outline (white line), and (c) with binary intracranial mask (sum of brain and CSF masks) outline.

noteworthy that although it had a significant effect on the segmentation of the simulated scan, its effect on the real scans was minimal. This is despite the larger influence of the partial volume effect due to the larger voxel size in the latter. This may reflect either the specificity of the subject's anatomy on which the digital atlas was based, or some effect of the MNI classification process.

Reproducibility experiments were performed to test the algorithm's stability and as a surrogate for a true *in vivo* gold standard. By limiting the interscan interval to a short interval (average 8 months), we introduced random variations in noise, head position and orientation, and voxel dimension, as well as some normal physiological variations (menstruation, body weight, etc.) while ensuring that any changes in brain and intracranial volumes were very small. In the control group, the TBV and ICV interscan reproducibility ($CR = 2 \times SD$ of the difference) were 35.2 and 29 cm^3 , respectively (2.8% and 1.98% of the mean baseline values), for the original pairs, and lower for the registered and matched scan pair comparisons, with 25.2 cm^3 and 17.06 cm^3 (2.02% and 1.16% of mean baseline values) for the latter. Absolute GM, WM, and CSF volume reproducibility values were similar to the TBV values for all scan pair comparisons, apart from a marked increase in dGMV for the registered-matched comparison compared to the unregistered result. Binary and CSF brain mask volume reproducibility values were similar to the IPD-derived values.

We expected a higher variability in the patients compared to the normal controls for all cerebral volumetric measures, in part due to ongoing biological processes (such as aging and possibly other processes associated with disease progression) and in part due to artifacts. For ICV, these effects should be reduced if one assumes that the shape and size of the cranium remain relatively unaltered over the interscan interval. The results confirmed these expectations, and we observed a general pattern of cerebral volume loss and CSF volume increase, and CR values roughly double those obtained for the controls. For ICV, the mean change and CR were very similar to the control values, with a very slight increase.

Visual inspection of the GM, WM, and CSF probability maps demonstrated the validity of our method. The most common segmentation error was the inclusion of small fragments of dura in the brain mask in the parieto-occipital region in approximately 10% of the subjects. This is prob-

ably due to the effect of gravity, which may reduce the gap between the brain and skull in that region as the subject lies supine. For the CSF, the comparison of the results with registration (Fig. 7, in particular the difference image) shows numerous inconsistencies. This reflects in part the difficulty of segmenting this component, because of its relatively low SNR. Furthermore, it is important to note that registration of the repeat scans is based on the brain alone, which is known to move relative to the cranium, causing changes in the distribution of CSF and rendering voxel-by-voxel comparison of the CSF segmentation across the scans meaningless. We found a slight benefit in reproducibility from scan pair matching.

There are several possible ways this algorithm could be improved. Although good agreement between the intensity histogram and fitted IPD was found, and the quality of the segmentation provides some justification for the use of the penta-Gaussian model, improved modeling of the partial volume effects (e.g., based on the uniform distribution) may provide more stable solutions (36). Local neighborhood information could be used to take into account genuine tissue intensity variations, and prevent the misclassification of WM-CSF boundary voxels as GM (e.g., Markov random field methods (16)). A possible initial approach that would take advantage of the algorithm's structure would be to use a combination of intensity information with boundary location to identify partial volume voxels.

In conclusion, we have demonstrated a new, fully automatic method to segment the brain and total intracranial CSF from T_1 volume scans with good accuracy and reproducibility. We envisage that this approach will be useful in a wide variety of applications in structural MRI and in combination with functional neuroimaging data such as PET and EEG.

ACKNOWLEDGMENTS

The authors thank Professor John Duncan for his support and input. We also thank Dave Brennan, of Glasgow University, for his help in implementing parts of the code, and Professor Robert Turner, of the Wellcome Department of Cognitive Neurology, UCL Institute of Neurology, for his assistance with the 2T data.

REFERENCES

- Maudgil DD, Free SL, Sisodiya SM, Lemieux L, Woermann FG, Fish DR, Shorvon SD. Identifying homologous anatomical landmarks on reconstructed magnetic resonance images of the human cerebral cortical surface. *J Anat* 1998;193:559–571.
- Lawson JA, Vogrin S, Bleasel AF, Cook MJ, Bye AM. Cerebral and cerebellar volume reduction in children with intractable epilepsy. *Epilepsia* 2000;41:1456–1462.
- Wilson M, Morgan PS, Lin X, Turner BP, Blumhardt LD. Quantitative diffusion weighted magnetic resonance imaging, cerebral atrophy, and disability in multiple sclerosis. *J Neurol Neurosurg Psychiatry* 2001;70:318–322.
- Fein G, Di Sclafani V, Tanabe J, Cardenas V, Weiner MW, Jagust WJ, Reed BR, Norman D, Schuff N, Kusdra L, Greenfield T, Chui H. Hippocampal and cortical atrophy predict dementia in subcortical ischemic vascular disease. *Neurology* 2000;55:1626–1635.
- Moran NF, Lemieux L, Kitchen ND, Fish DR, Shorvon SD. Extrahippocampal temporal lobe atrophy in temporal lobe epilepsy and mesial temporal sclerosis. *Brain* 2001;124:167–175.
- Liu R, Lemieux L, Bell G, Shorvon SD, Sisodiya SM, Sander JWAS, Duncan JS. A longitudinal quantitative MRI study of community-based patients with chronic and newly diagnosed seizures: methodology and preliminary findings. *NeuroImage* 2001;14:231–243.
- Labbé C, Koepp M, Ashburner J, Spinks T, Richardson M, Duncan J, Cunningham V. Absolute PET quantification with correction for partial volume effects within cerebral structures. In: Carson C, Daube-Witherspoon M, Herscovitch P, editors. *Quantitative functional brain imaging with positron emission tomography*. San Diego: Academic Press; 1998. p 59–66.
- Aston JAD, Cunningham VJ, Hammers A, Lemieux L, Gunn RN. Partial volume correction: a recipe. *Neuroimage* 2002;16:S74.
- Wagner M, Fuchs M, Wischmann HA, Ottenberg K, Dössel O. Cortex segmentation from 3D MR images for MEG reconstructions. In: Baumgartner C, Deecke L, Stroing G, Williamson SJ, editors. *Biomagnetism: fundamental research and clinical applications*. Amsterdam: Elsevier Science IOS Press; 1995. p 433–438.
- Lemieux L, Wieshmann UC, Moran NF, Fish DR, Shorvon SD. The detection and significance of subtle changes in mixed-signal brain lesions by serial MRI scan matching and spatial normalization. *Med Image Anal* 1998;2:227–242.
- Lemieux L, Liu R, Duncan JD. Hippocampal and cerebellar volumetry in serially acquired MRI volume scans. *Magn Reson Imaging* 2000;18:1027–1033.
- Calmon G, Roberts N. Automatic measurements of changes in brain volume on consecutive 3D MR images by segmentation propagation. *Magn Reson Imaging* 2000;18:439–453.
- Liu RSN, Lemieux L, Shorvon SD, Sisodiya SM, Sander JWAS, Bell G, Duncan JS. Increase in brain size with abstinence from alcohol. *Lancet* 2000;355:1969–1970.
- Alfano B, Brunetti A, Covelli EM, Quarantelli M, Panico MR, Ciarmiello A, Salvatore M. Unsupervised, automated segmentation of the normal brain using a multispectral relaxometric magnetic resonance approach. *Magn Reson Med* 1997;37:84–93.
- Bedell BJ, Narayana PA. Volumetric analysis of white matter, grey matter, and CSF using fractional volume analysis. *Magn Reson Med* 1998;39:961–969.
- Held K, Kops ER, Krause BJ, Wells III WM, Kikinis R, Muller-Gartner HW. Markov random field segmentation of brain MR images. *IEEE Med Imaging* 1997;16:878–886.
- Herndon RC, Lancaster JL, Giedd JN, Fox PT. Quantification of white matter and grey matter volumes from three-dimensional magnetic resonance volume studies using fuzzy classifiers. *J Magn Reson Imaging* 1998;8:1097–1105.
- Pham DL, Prince JL. An adaptive fuzzy segmentation algorithm for three-dimensional magnetic resonance images. In: Kuba A, Samal M, Todd-Pokropek A, editors. *Image processing in medical imaging*. In: Proceedings of the 16th International Conference of IPMI, Berlin, 1999. p 140–153.
- Shattuck DW, Sandor-Leahy SR, Schaper KA, Rottenberg DA, Leahy RM. Magnetic resonance image tissue classification using a partial volume model. *Neuroimage* 2001;13:856–876.
- Brummer ME, Mersereau RM, Eisner RL, Lewine RR. Automatic detection of brain contours in MRI data sets. *IEEE Trans Med Imaging* 1993;12:153–166.
- Sandor S, Leahy R. Surface-based labeling of cortical anatomy using a deformable atlas. *IEEE Trans Med Imaging* 1997;16:41–54.
- Lemieux L, Hagemann G, Krakow K, Woermann FG. Fast, accurate and reproducible automatic segmentation of the brain in T1-weighted volume magnetic resonance image data. *Magn Reson Med* 1999;42:127–135.
- Dawant BM, Hartman SL, Thirion JP, Vandermeulen D, Demaerel P. Automatic 3-D segmentation of internal structures of the head in MR images using a combination of similarity and free-form transformations. I. Methodology and validation on normal subjects. *IEEE Trans Med Imaging* 1999;18:909–916.
- Grabowski TJ, Frank RJ, Szumski NR, Brown CK, Damasio H. Validation of partial tissue segmentation of single-channel magnetic resonance images of the brain. *Neuroimage* 2000;12:640–656.
- Wang D, Dordrell DM. MR image-based measurement of rates of change in volumes of brain structures. I. Method and validation. *Magn Reson Imaging* 2002;20:27–40.
- Sled JG, Zijdenbos AP, Evans AC. A nonparametric method for automatic correction of intensity nonuniformity in MRI data. *IEEE Trans Med Imaging* 1998;17:87–97.
- Arnold JB, Liow JS, Schaper KA, Stern JJ, Sled JG, Shattuck DW, Worth AJ, Cohen MS, Leahy RM, Mazziotta JC, Rottenberg DA. Qualitative and quantitative evaluation of six algorithms for correcting intensity nonuniformity effect. *NeuroImage* 2001;13:931–943.
- Gudbjartsson H, Patz S. The Rician distribution of noisy MRI data. *Magn Reson Med* 1995;34:910–914.
- Sonka M, Hlavac V, Boyle R. *Image processing, analysis and machine vision*. London: Chapman & Hall; 1993.
- Collins DL, Zijdenbos AP, Baare WFC, Evans AC. ANIMAL+INSECT: improved cortical structures segmentation. In: Kuba A, Samal M, Todd-Pokropek A, editors. *Image processing in medical imaging*. In: Proceedings of the 16th International Conference of IPMI, Berlin, 1999. p 210–223.
- Collins DL, Zijdenbos AP, Kollokian V, Sled JG, Kabani NJ, Holmes CJ, Evans AC. Design and construction of a realistic digital brain phantom. *IEEE Trans Med Imaging* 1998;17:463–468.
- Wieshmann UC, Free SL, Stevens JM, Shorvon SD. Image contrast and hippocampal volumetric measurements. *Magn Reson Imaging* 1998;16:13–17.
- Lemieux L, Barker GJ. Measurement of small inter-scan fluctuations in voxel dimensions in magnetic resonance images using registration. *Med Phys* 1998;25:1049–1054.
- Bland JM, Altman DG. Statistical methods for assessing agreement between two methods of clinical measurement. *Lancet* 1996;327:307–310.
- Crum WR, Scapill RI, Fox NC. Automated hippocampal segmentation by regional fluid registration of serial MRI: validation and application in Alzheimer's disease. *NeuroImage* 2001;13:847–855.
- Santago P, Gage HD. Quantification of MR brain images by mixture density and partial volume modeling. *IEEE Trans Med Imaging* 1993;12:566–574.